

# Constrained velocity-free control of spacecraft attitude via explicit reference governor

Qingqing Dang<sup>a</sup>, Wenbo Li<sup>b,\*</sup>, Haichao Gui<sup>c</sup>

<sup>a</sup>*School of Civil Aviation, Northwestern Polytechnical  
University, Xi'an, 710072, Shanxi, China*

<sup>b</sup>*Beijing Institute of Control Engineering, China Academy of Space  
Technology, Beijing, 100190, China*

<sup>c</sup>*School of Astronautics, Beihang University, Beijing, 100191, China*

---

## Abstract

This paper introduces an explicit reference governor-based control scheme tailored for addressing the velocity-free spacecraft attitude maneuver problem. This problem is subject to specific constraints, namely the pointing constraint, angular velocity constraint, and input saturation. The proposed control scheme operates in two layers, ensuring the asymptotic stability of the spacecraft's attitude while adhering to the aforementioned constraints. The inner layer employs output feedback control utilizing an angular velocity observer based on immersion and invariance technology. This observer facilitates attitude stabilization without the measurement of angular velocity. Through an analysis of the geometry associated with the pointing constraint, determination of the upper bound of angular velocity, and optimization of the control input solution, the reference layer establishes a safety boundary described by the invariant set. Additionally, we introduce the dynamic factor related to the angular velocity estimation error into the invariant set to prevent states from exceeding the constraint set due to unmeasurable angular velocity information. The shortest guidance path is then designed in the reference layer. Finally, we substantiate the efficacy of the proposed constrained attitude control algorithm through numerical simulations.

*Keywords:*

---

\*

\*Corresponding author

*Email address:* liwenbo\_502@163.com (Wenbo Li)

## 1. Introduction

Spacecraft attitude maneuver plays a significant role in complex space autonomous missions[1]. Restricted by the actuators and sensitive payloads, attitude maneuver algorithms must ensure system stability while simultaneously adhering to multiple constraints [2, 3, 4]. For instance, the spacecraft is usually required to maneuver from one state to another within the defined time , while keeping its star sensor avoid from the bright objects (e.g. earth) and preventing the command torque from exceeding the capacity of the actuator [5]. These missions exemplify spacecraft maneuvering amidst state and control constraints [6, 7]. Moreover, in scenarios where gyroscopes fail, the unavailability of angular velocity information becomes a significant challenge [8]. Consequently, constrained velocity-free attitude control is an issue of great theoretical and practical importance.

For attitude control systems with actuator saturation, if the input constraints are not considered in the controller design explicitly, although the performance is affected by the input limitation, its stability sometimes can still be proved theoretically [9]. Traditional controllers designed directly through Lyapunov function lack the ability to restrict state trajectories. Hence, the attitude commands are used in the attitude maneuver path design in the presence of multiple attitude constraints [5, 10]. This strategy can effectively solve part of the engineering problems, but it suffers from limited flexibility and struggles to meet tasks demanding high real-time dynamic requirements. Addressing challenges caused by actuator saturation, control bandwidth limits, slew rate constraints, and/or eigenaxis slew constraints, Wie et al. introduced saturation and integration functions within a nonlinear feedback control logic for rapid re-targeting control of agile spacecraft [11]. This method can handle single-axis maneuvers with particular constraints well. However, it encounters difficulties in handling three-axis maneuvers with intricate constraints.

The amalgamation of potential functions and Lyapunov functions presents a promising technology for addressing complex constraints in the constrained attitude control problem [12, 13, 14]. Lee et al. [15] constructed a strictly convex logarithmic barrier potential for attitude-constrained zones by utilizing a convex parameterization technology. Inspired by[15] and using the

anti-unwinding attitude error function, a new algorithm for the attitude re-orientation guidance under forbidden pointing constraints is proposed in [16]. Furthermore, Shen et al. [17] addressed the rest-to-rest three-axis attitude reorientation under multiple attitude-constraint zones and angular velocity limits via a quadratic potential function and a logarithmic potential function. Nevertheless, it is difficult to simultaneously handle different types of complex constraints by the potential functions based constrained control algorithm. Since the potential function is constructed in the Lyapunov function and the convergence of Lyapunov function is the result of the convergence game between potential function and states, the robustness of the system may become worse.

Trajectory optimization methods, notably model predictive control (MPC), offer a means to tackle constrained control issues. In [18] and [19], MPC on  $SO(3)$  has been developed for constrained attitude maneuver of fully actuated spacecraft. However, the necessity to optimize the function at each sampling horizon in MPC restricts its application in systems requiring rapid response, such as spacecraft maneuvering. Recently, a novel add-on control scheme called explicit reference governor (ERG) was introduced by Nicotra et al. [20, 21, 22, 23]. The key idea is to augment a pre-stabilized system with a control unit and manipulates the auxiliary reference to ensure constraint satisfaction, which means the stability and the constraint issues can be handled separately. This control technology has found application in solving problems related to Unmanned Aerial Vehicles and spacecraft attitude control with state constraints [3, 7, 24, 25].

In addition to constraints, another challenge in attitude control is the velocity-free control problem. This issue has drawn significant attention from researchers and has been extensively studied [26, 27, 28]. For instance, immersion and invariance (I&I) technology have been utilized to develop a globally exponentially convergent observer for the angular velocity in [9, 27, 29, 30]. In our earlier research, a six-degree-of-freedom observer was constructed using the I&I approach [31]. However, the velocity-free attitude maneuver problem in the presence of constraints was studied in just a few works. For instance, a velocity-free attitude reorientation control law with pointing constraints is established in [32].

Inspired by the ERG and the I&I technologies, a constrained velocity-free control algorithm for spacecraft reorientation is presented in this paper. The algorithm takes into account attitude pointing, angular velocity, and control input constraints. The formulation of attitude dynamics and vari-

ous constraints is expressed using modified Rodrigues parameters (MRPs). The MRPs constitute a singular, nonunique and minimal parametrization set of the three-dimensional special orthogonal group  $\text{SO}(3)$ . Fortunately, the singularity can be avoided by using the nonuniqueness properties through switching the parameters between MRPs and its shadow at the unit sphere [33, 34]. Subsequently, the ERG-based control scheme is derived, wherein the output controller, relying on the angular velocity observer, is primarily designed in the inner loop. To the best of the authors' knowledge, the result presented in this paper is the first attempt to address the observer-based attitude maneuver issue with pointing constraints, angular velocity constraints, and input constraints. Finally, the performance and robustness of the proposed algorithm is verified by the numerical simulations and Monte Carlo simulations.

## 2. Preliminaries

### 2.1. Spacecraft attitude kinematics and dynamics

The MRPs vector is defined in terms of an Euler rotation angle  $\phi \in \mathbb{R}$  about the principal axis  $\{\mathbf{n} | \mathbf{n}^T \mathbf{n} = 1, \mathbf{n} \in \mathbb{R}^3\}$ . Let  $\mathcal{F}_B$  be the body-fixed frame, and  $\mathcal{F}_I$  be the inertial frame. Then, the attitude with respect to the inertial frame can be described by MPRs and given by  $\boldsymbol{\sigma}_{BI} = \mathbf{n}_{BI} \tan(\phi_{BI}/4)$ . The attitude kinematics and dynamics of the rigid-body spacecraft are given by [35]

$$\dot{\boldsymbol{\sigma}}_{BI} = G(\boldsymbol{\sigma}_{BI}) \boldsymbol{\omega}_{BI}^B \quad (1a)$$

$$G(\boldsymbol{\sigma}_{BI}) = \frac{1}{2} \left( \frac{1 - \boldsymbol{\sigma}_{BI}^T \boldsymbol{\sigma}_{BI}}{2} \mathbf{I}_3 + \boldsymbol{\sigma}_{BI}^\times + \boldsymbol{\sigma}_{BI} \boldsymbol{\sigma}_{BI}^T \right)$$

$$\mathbf{J} \dot{\boldsymbol{\omega}}_{BI}^B + \boldsymbol{\omega}_{BI}^B \times \mathbf{J} \boldsymbol{\omega}_{BI}^B = \boldsymbol{\tau}_c^B + \boldsymbol{\tau}_d^B \quad (1b)$$

where  $\boldsymbol{\omega}_{BI}^B \in \mathbb{R}^3$  denotes the angular velocity expressed in the body-fixed frame,  $\mathbf{J} \in \mathbb{R}^{3 \times 3}$  is the inertia matrix,  $\mathbf{I}_3$  denotes the identity matrix, and  $(\mathbf{x})^\times$  is the  $3 \times 3$  skew-symmetric cross-product matrix associated with vector  $\mathbf{x} \in \mathbb{R}^3$ .  $\boldsymbol{\tau}_c^B$  and  $\boldsymbol{\tau}_d^B$  represent the control torque and the disturbance, respectively.

$\boldsymbol{\sigma}_{XY}$  denotes the orientation of  $X$  frame relative to  $Y$  frame.  $\omega_{YZ}^X$  is the angular velocity of  $Y$  frame relative to  $Z$  frame expressed in  $X$  frame. Then,

the relative attitude between two frames is defined as

$$\boldsymbol{\sigma}_{XY} = \frac{\boldsymbol{\sigma}_{YI}(\boldsymbol{\sigma}_{XI}^T \boldsymbol{\sigma}_{XI} - 1) + \boldsymbol{\sigma}_{XI}(1 - \boldsymbol{\sigma}_{YI}^T \boldsymbol{\sigma}_{YI}) - 2\boldsymbol{\sigma}_{YI}^\times \boldsymbol{\sigma}_{XI}}{1 + \boldsymbol{\sigma}_{XI}^T \boldsymbol{\sigma}_{XI} \boldsymbol{\sigma}_{YI}^T \boldsymbol{\sigma}_{YI} + 2\boldsymbol{\sigma}_{YI}^T \boldsymbol{\sigma}_{XI}}$$

and the dynamics of  $\boldsymbol{\sigma}_{XY}$  is given by

$$\dot{\boldsymbol{\sigma}}_{XY} = G(\boldsymbol{\sigma}_{XY})\boldsymbol{\omega}_{XY}^X \quad (2a)$$

$$\mathbf{J}\dot{\boldsymbol{\omega}}_{XY}^X + \boldsymbol{\omega}_{XI}^X \times \mathbf{J}\boldsymbol{\omega}_{XI}^X - \mathbf{J}(\boldsymbol{\omega}_{XY}^X \times \boldsymbol{\omega}_{YI}^X - \mathbf{C}_Y^X \dot{\boldsymbol{\omega}}_{YI}^Y) = \boldsymbol{\tau}_c^B \quad (2b)$$

where  $\boldsymbol{\omega}_{XY}^X = \boldsymbol{\omega}_{XI}^X - \boldsymbol{\omega}_{YI}^X$  and  $\boldsymbol{\omega}_{YI}^X = \mathbf{C}_Y^X \boldsymbol{\omega}_{YI}^Y$ . The rotation matrix in terms of the MRPs from  $Y$  frame to  $X$  frame can be expressed as

$$\mathbf{C}_Y^X = \mathbf{I}_3 + \frac{8(\boldsymbol{\sigma}_{XY}^\times)^2 - 4(1 - \boldsymbol{\sigma}_{XY}^T \boldsymbol{\sigma}_{XY})\boldsymbol{\sigma}_{XY}^\times}{(1 + \boldsymbol{\sigma}_{XY}^T \boldsymbol{\sigma}_{XY})^2} \quad (3)$$

The following properties will be frequently used in this paper:

$$\boldsymbol{\sigma}_{XY}^T G(\boldsymbol{\sigma}_{XY}) = \left( \frac{1 + \boldsymbol{\sigma}_{XY}^T \boldsymbol{\sigma}_{XY}}{4} \right) \boldsymbol{\sigma}_{XY}^T \quad (4)$$

$$G(\boldsymbol{\sigma}_{XY})^T G(\boldsymbol{\sigma}) = \left( \frac{1 + \boldsymbol{\sigma}^T \boldsymbol{\sigma}}{4} \right)^2 \mathbf{I}_3 \quad (5)$$

According to the description of MRPs in [33], MRPs have geometric singularities when  $\phi = \pm 360^\circ$ , and it is not unique because of the shadow set, i.e.,  $\boldsymbol{\sigma} = \boldsymbol{\sigma}^s, \boldsymbol{\sigma}^s = -\boldsymbol{\sigma}/\boldsymbol{\sigma}^T \boldsymbol{\sigma}$ . Recalling the definition of  $\boldsymbol{\sigma}$ , one knows that  $\|\boldsymbol{\sigma}\| \leq 1$  for all  $|\phi| \leq 180^\circ$ . Thus, the spacecraft attitude can be globally parameterized with the shortest principal rotation by switching the  $\boldsymbol{\sigma}$  and  $\boldsymbol{\sigma}^s$  at the unit sphere  $\|\boldsymbol{\sigma}\| = 1$ . Consequently, we stipulate that the magnitude of  $\boldsymbol{\sigma}$  is bounded by 1, i.e.,  $\|\boldsymbol{\sigma}\| \leq 1$ , which is suited to describe any reorientation.

## 2.2. State and control constraints

The pointing constraint, the angular velocity constraint and the input limitation are considered in this paper. For the pointing constraint, we suppose the instantaneous angle  $\vartheta$  between a body-fixed unit vector  $\mathbf{r}_c^B$  (such as cameras) and a inertial constant unit vector  $\mathbf{r}_t^I$  (observed target) should be maintained in a half-cone angel  $\vartheta_m$ , i.e.,  $\theta \leq \vartheta_m$ , which is equivalent to

$$\mathcal{C}_p = \left\{ (\boldsymbol{\sigma}_{BI}, \boldsymbol{\omega}_{BI}^B) : \mathbf{r}_c^B \cdot \mathbf{r}_t^B \geq \cos(\vartheta_m), \vartheta_m \in (0, \frac{\pi}{2}) \right\} \quad (6)$$

where  $\mathbf{r}_t^B = \mathbf{C}_I^B \mathbf{r}_t^I$  is the expression of  $\mathbf{r}_t^I$  in  $\mathcal{F}_B$ .

In consideration of the payload requirements, the angular velocity constraint is always exists. Then the constraint set is given by

$$\mathcal{C}_\omega = \{(\boldsymbol{\sigma}_{BI}, \boldsymbol{\omega}_{BI}^B) : \|\boldsymbol{\omega}_{BI}^B\| \leq \omega_{\max}, \omega_{\max} > 0\} \quad (7)$$

where  $\omega_{\max} \in \mathbb{R}^+$  is the maximum angular velocity amplitude.

The angular momentum exchange devices such as reaction wheels and control moment gyros are usually used as the spacecraft attitude control actuators. These devices may be saturated when the command torque is large. For simplicity, the actuator constraint is formulated as

$$\mathcal{C}_\tau = \{(\boldsymbol{\sigma}_{BI}, \boldsymbol{\omega}_{BI}^B) : \|\boldsymbol{\tau}_c^B\| \leq \tau_{\max}, \tau_{\max} > 0\} \quad (8)$$

where  $\tau_{\max} \in \mathbb{R}^+$  is the maximum allowable control torque.

Finally, the dynamic safety margin of the system is the intersection of the aforementioned three subsets:

$$\mathcal{C} = \mathcal{C}_p \cap \mathcal{C}_\omega \cap \mathcal{C}_\tau \quad (9)$$

### 2.3. Problem statements

This paper aims to develop a ERG control scheme that drives the system states  $(\boldsymbol{\sigma}_{BI}, \boldsymbol{\omega}_{BI}^B)$  to the desired equilibrium  $(\boldsymbol{\sigma}_{DI}, \mathbf{0}_{3 \times 1})$  while satisfying the constraints (6), (7), and (8). The proposed ERG-based control structure (shown in Fig. 1) consists of two cascaded control units. The primary controller is given by an angular velocity observer-based output feedback controller, which is able to pre-stabilize the unconstrained system to an auxiliary reference  $\boldsymbol{\sigma}_{VI}$ . The reference governor (navigation layer) unit is designed to guarantee the constraint enforcement by manipulating the kinematics of  $\boldsymbol{\sigma}_{VI}$ . Clearly, the asymptotic convergence property of the closed-loop control system will be achieved by the goal that auxiliary reference  $\boldsymbol{\sigma}_{VI}$  asymptotically tends to  $\boldsymbol{\sigma}_{DI}$ . The reference attitude  $\boldsymbol{\sigma}_{DI}$  remains constant and is chosen within the admissible region, i.e., equation (6) holds true when  $\boldsymbol{\sigma}_{BI} = \boldsymbol{\sigma}_{DI}$ .

## 3. Primary controller design

This section proposes an angular velocity-free control law so as to stabilize the attitude toward a constant reference  $\bar{\boldsymbol{\sigma}}_{VI}$  ( $\dot{\boldsymbol{\sigma}}_{VI} = \mathbf{0}_{3 \times 1}$ ) when the constraints and disturbance are neglected ( $\boldsymbol{\tau}_d = \mathbf{0}_{3 \times 1}$ ). The time variation of  $\boldsymbol{\sigma}_{VI}$  will be addressed by the reference management unit, which is detailed in the next section.

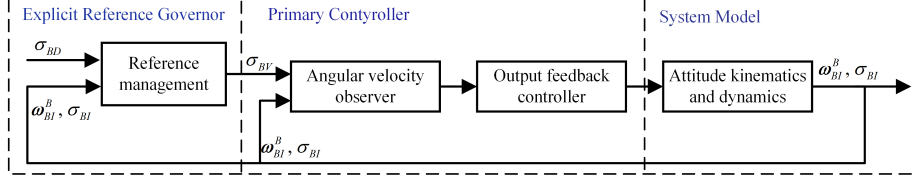


Figure 1: The architecture of the explicit reference governor based attitude control scheme.

### 3.1. Angular velocity observer design

The angular velocity observer is constructed based on the I&I theory [30, 31]. Let  $\mathcal{F}_E$  be the estimation frame of the  $\mathcal{F}_B$ . The attitude and angular estimation errors in terms of MRPs are given by

$$\sigma_{BE} = \frac{\sigma_{EI}(\sigma_{BI}^T \sigma_{BI} - 1) + \sigma_{BI}(1 - \sigma_{EI}^T \sigma_{EI}) - 2\sigma_{EI}^\times \sigma_{BI}}{1 + \sigma_{BI}^T \sigma_{BI} \sigma_{EI}^T \sigma_{EI} + 2\sigma_{EI}^T \sigma_{BI}} \quad (10a)$$

$$\omega_{BE}^B = \omega_{BI}^B - C_E^B \omega_{EI}^E = \omega_{BI}^B - \omega_{EI}^B \quad (10b)$$

To ensure  $\omega_{BE}^B \rightarrow 0$  and  $\sigma_{BE} \rightarrow 0$ , a scalar  $\varpi \in \mathbb{R}^+$  that can 'cover' the  $\omega_{EI}^B$  is introduced as

$$\varpi = \sqrt{\varepsilon_\omega + \|\omega_{EI}^B\|^2} \quad (11)$$

where  $\varepsilon_\omega \in \mathbb{R}^+$  is a constant to be selected, which is utilized to ensure the existence of the time derivative of  $\varpi$ . Then,  $\omega_{EI}^B$  is generated by

$$\omega_{EI}^B = \xi + 4\mathbf{J}^{-1}\beta(\underline{\varpi})\sigma_{BE} \quad (12)$$

where  $\underline{\varpi}$  is the estimate of  $\varpi$ ,  $\xi$  and  $\beta(\underline{\varpi})$  are the parameter related to  $\omega_{EI}^B$  and a function of  $\underline{\varpi}$ , respectively. The dynamics of  $\xi$ ,  $\underline{\varpi}$ , and  $\sigma_{EI}$  are designed as

$$\begin{aligned} \dot{\xi} = & \mathbf{J}^{-1}(-\omega_{EI}^B \times \mathbf{J}\omega_{EI}^B + \tau_c^B) - 4\mathbf{J}^{-1}\dot{\beta}(\underline{\varpi})\sigma_{BE} \\ & - 4\mathbf{J}^{-1}\beta(\underline{\varpi})\dot{\sigma}_{1BE} \end{aligned} \quad (13a)$$

$$\dot{\underline{\varpi}} = \underline{\varpi}^{-1}(\omega_{EI}^B)^T \mathbf{J}^{-1}(-\omega_{EI}^B \times \mathbf{J}\omega_{EI}^B + \tau_c^B) - K_{\underline{\varpi}}(\underline{\varpi} - \varpi) \quad (13b)$$

$$\dot{\sigma}_{EI} = G(\sigma_{EI})(\omega_{EI}^E + K_\sigma C_B^E \sigma_{BE}) \quad (13c)$$

where  $K_{\underline{\varpi}}$  and  $K_\sigma$  are the dynamic gains to be designed,  $\dot{\boldsymbol{\sigma}}_{1BE}$  represents part of the dynamics of  $\boldsymbol{\sigma}_{BE}$ , and it can be obtained from (1a), (10b), and (13c) :

$$\begin{aligned}
\dot{\boldsymbol{\sigma}}_{BE} &= G(\boldsymbol{\sigma}_{BE})(\boldsymbol{\omega}_{BI}^B - \boldsymbol{\omega}_{EI}^B) \\
&= G(\boldsymbol{\sigma}_{BE})[\boldsymbol{\omega}_{BI}^B - \mathbf{C}_E^B(\boldsymbol{\omega}_{EI}^E + K_\sigma \mathbf{C}_B^E \boldsymbol{\sigma}_{BE})] \\
&= G(\boldsymbol{\sigma}_{BE})(\boldsymbol{\omega}_{BE}^B - K_\sigma \boldsymbol{\sigma}_{BE}) \\
&= \dot{\boldsymbol{\sigma}}_{1BE} + \dot{\boldsymbol{\sigma}}_{2BE}
\end{aligned} \tag{14}$$

with  $\dot{\boldsymbol{\sigma}}_{1BE} = -G(\boldsymbol{\sigma}_{BE})K_\sigma \boldsymbol{\sigma}_{BE}$  and  $\dot{\boldsymbol{\sigma}}_{2BE} = G(\boldsymbol{\sigma}_{BE})\boldsymbol{\omega}_{BE}^B$ .

To inject the nonlinear terms in the dynamics of  $\boldsymbol{\omega}_{BE}^B$  a dynamic scaling technique is introduced:

$$\mathbf{z} = \frac{\boldsymbol{\omega}_{BE}^B}{r} \tag{15}$$

where  $r$  is the dynamic scaling factor and is updated by the following law

$$\dot{r} = \frac{r}{J_m}(J_M \|\underline{\varpi} - \underline{\varpi}\|) - \frac{k_r}{J_M}(r - 1) \tag{16}$$

where  $k_r \in \mathbb{R}^+$  is the dynamic scaling gain to be determined,  $J_m$  and  $J_M$  are the minimum and the maximum eigenvalues of the inertia matrix  $\mathbf{J}$ , respectively. If  $r(t) = 1$ ,  $\dot{r} \geq 0$ . Hence, it satisfies  $r(t) \geq 1$  for all  $t \geq 0$  when  $r(0) \geq 1$ . Finally, the convergence analysis of the proposed observer (12) is summarized as the following proposition.

**proposition 1.** *Consider the angular velocity observer in (12) with dynamics given in (13), (16), and the gains are given as*

$$\beta(\underline{\varpi}) = 4\underline{\beta}(\underline{\varpi})G^T(\boldsymbol{\sigma}_{BE}) \tag{17a}$$

$$\underline{\beta}(\underline{\varpi}) = J_M \|\underline{\varpi}\| + \frac{J_m k_r}{J_M} + 1 + \rho_\varpi \tag{17b}$$

$$K_{\underline{\varpi}} = 8 \left( \frac{\|\boldsymbol{\omega}_{EI}^B\| \beta(\underline{\varpi}) r}{J_m} \right)^2 + \frac{1}{2} r^2 J_M + \rho_{\underline{\varpi}} \tag{17c}$$

$$K_\sigma = \frac{1}{2} r^2 + \rho_\sigma \tag{17d}$$

$$k_r = \frac{1}{2} \frac{J_M^2}{J_m} + \rho_r \tag{17e}$$

where  $\rho_{\varpi}$ ,  $\rho_{\underline{\varpi}}$ ,  $\rho_{\sigma}$ , and  $\rho_r$  are positive constants that can be tuned for different convergence rates of the estimation errors. Then, the dynamic scaling factor  $r$  is bounded and the errors globally exponentially converges to the origin, i.e.,  $\lim_{t \rightarrow \infty} e^{\alpha t} \|\boldsymbol{\omega}_{BE}^B\| = 0, \alpha \in \mathbb{R}^+$ .

**Proof:** See the Appendix. ■

### 3.2. Velocity-free controller design

The aforementioned angular velocity observer is used to derive a velocity-free feedback attitude controller. As shown in Fig. 1, the following theorem summarize the result on the unconstrained output controller.

**Theorem 1.** *Consider the attitude dynamics given in (1) and the angular velocity observer given in (12)-(17). Then, the output feedback control law is given by*

$$\boldsymbol{\tau}_c^B = -k_p \boldsymbol{\sigma}_{BV} - k_d \boldsymbol{\omega}_{EI}^B \quad (18)$$

with  $k_p, k_d > 0$ , the equilibrium  $(\bar{\boldsymbol{\sigma}}_{VI}, \mathbf{0}_{3 \times 1})$  is asymptotically stable within the admissible set, i.e.,  $\lim_{t \rightarrow \infty} (\boldsymbol{\sigma}_{BI}, \boldsymbol{\omega}_{BI}^B) = (\bar{\boldsymbol{\sigma}}_{VI}, \mathbf{0}_{3 \times 1})$ .

**Proof:** By employing (10b), the control law (18) can be expressed as a full-state controller augmented by perturbations resulting from velocity estimation errors, namely,

$$\boldsymbol{\tau}_c^B = -k_p \boldsymbol{\sigma}_{BV} - k_d \boldsymbol{\omega}_{BI}^B + k_d \boldsymbol{\omega}_{BE}^B \quad (19)$$

Consider a Lyapunov function candidate as follows:

$$V_c = 2k_p \ln(1 + \boldsymbol{\sigma}_{BV}^2) + \frac{1}{2} (\boldsymbol{\omega}_{BI}^B)^T \mathbf{J} \boldsymbol{\omega}_{BI}^B \quad (20)$$

Taking the time derivative of (20) along (1), (4), and (19), one can obtain

$$\begin{aligned} \dot{V}_c &= 4k_p \frac{\boldsymbol{\sigma}_{BV}^T \dot{\boldsymbol{\sigma}}_{BV}}{1 + \boldsymbol{\sigma}_{BV}^2} + (\boldsymbol{\omega}_{BI}^B)^T \mathbf{J} \dot{\boldsymbol{\omega}}_{BI}^B \\ &\leq -k_d \|\boldsymbol{\omega}_{BI}^B\|^2 + k_d \|\boldsymbol{\omega}_{BI}^B\| \|\boldsymbol{\omega}_{BE}^B\| \end{aligned} \quad (21)$$

Clearly,  $\dot{V}_c$  contains a term with indefinite sign induced by angular velocity estimation error. To eliminate this effect, consider a positive definite Lyapunov function in the following form:

$$V = V_c + \delta_z V_z \quad (22)$$

where  $\delta_z$  is a positive constant to be determined. Differentiating  $V$  and applying (21) and (A.4) yields

$$\begin{aligned} \dot{V} &\leq -k_d \|\boldsymbol{\omega}_{BI}^B\|^2 + k_d \|\boldsymbol{\omega}_{BI}^B\| \|\boldsymbol{\omega}_{BE}^B\| - \delta_z (1 + \rho_\varpi) \|\mathbf{z}\|^2 \\ &\leq - \left[ \|\boldsymbol{\omega}_{BI}^B\| \|\boldsymbol{\omega}_{BE}^B\| \right] \begin{bmatrix} k_d & -\frac{1}{2}k_d \\ -\frac{1}{2}k_d & \delta_z r^{-2} (1 + \rho_\varpi) \end{bmatrix} \begin{bmatrix} \|\boldsymbol{\omega}_{BI}^B\| \\ \|\boldsymbol{\omega}_{BE}^B\| \end{bmatrix} \end{aligned} \quad (23)$$

Given that  $1 \leq r < \infty$ , there exists a sufficiently large  $\delta_z$  such that  $\dot{V}$  is negative semi-definite for  $\bar{\boldsymbol{\sigma}}_{VI}$ . By using the LaSalle invariance principle, one can conclude that the equilibrium point  $(\bar{\boldsymbol{\sigma}}_{VI}, \mathbf{0}_{3 \times 1})$  of the system is asymptotically stable. This completes the proof. ■

Obviously,  $\boldsymbol{\sigma}_{VI}$  is time varying, **Theorem 1** addresses the claim concerning the tracking error stability of  $\bar{\boldsymbol{\sigma}}_{VI}$  rather than  $\boldsymbol{\sigma}_{VI}$ . In fact, since the final state  $\boldsymbol{\sigma}_{DI}$  is a constant attitude, the inner loop controller only needs to ensure that the attitude can converge to the final state. Additionally, the precise acquisition of angular velocity is challenging, resulting in difficulties in strictly guaranteeing the angular velocity constraint. Fortunately, the value of the dynamic scaling factor  $r$  reflects the estimation error. By designing functions associated with  $r$ , it becomes possible to satisfy the angular velocity constraints. These properties will be utilized in the subsequent section.

**Remark 1.** Throughout the preceding analysis, it is evident that the design of the output feedback controller remains independent of the angular velocity observer (refer to (18) and (19)), which greatly reduces the difficulty of the controller design. Moreover, (13) and (17) suggest a conflict between the scale of the observer gains and system robustness. However, there are always parameter uncertainties in practical missions, so it is necessary to balance the two properties, which will be verified in detail in the simulation.

#### 4. Reference management

The reference management layer of ERG (illustrated in Fig. 1) devises an auxiliary control law that manipulates the reference state towards the

primary stabilized system [36, 20]. The objective of this section is to handle the constraints outlined in (6) – (8) by designing the safety margin and the navigation field, which is achieved by the invariant set in the Lyapunov function centered on the reference state  $\sigma_{VI}$ . The formulation of the auxiliary reference takes the following form:

$$\dot{\sigma}_{VI} = \Delta(\sigma_{BV}, \boldsymbol{\omega}_{EI}^B) \chi(\sigma_{VI}, \sigma_{VD}) \quad (24)$$

where  $\Delta(\sigma_{BV}, \boldsymbol{\omega}_{EI}^B) : \mathbb{R}^3 \times \mathbb{R}^3 \rightarrow \mathbb{R}$  is the dynamic safety margin that indicates how safe it is within the allowable set.  $\chi(\sigma_{VI}, \sigma_{VD}) : \mathbb{R}^3 \times \mathbb{R}^3 \rightarrow \mathbb{R}^3$  denotes the navigation field of the current state  $\sigma_{VI}$ , and the  $\sigma_{VD}$  is utilized to drive the  $\sigma_{VI}$  towards to  $\sigma_{DI}$ .

#### 4.1. Safety margin

From an intuitive perspective, the safety margin can be treated as the distance between the constraint boundary and the navigation field. Since  $\dot{V}$  is negative semi-definite (see (23)), the forward invariant set  $\{(\boldsymbol{\sigma}_{BI}, \boldsymbol{\omega}_{BI}^B) : V \leq \Gamma\}$  can be used to design the safety margin, where the upper bound  $\Gamma(\boldsymbol{\sigma}_{VI}^V, \boldsymbol{\omega}_{VI}^V)$  is determined by the constraints (6) – (8). In [21] and [22], authors design the dynamic safety margin in the form  $\Delta(\sigma_{BV}, \boldsymbol{\omega}_{EI}^B) = k_e(\Gamma - V)$ , where the constant  $k_e$  is used to adjust the dynamic performance. Unfortunately, since the exact estimation error  $\boldsymbol{\omega}_{BE}^B$  is unavailable, the angular velocity can not be obtained either. In order to prevent  $\Delta$  being negative caused by  $\boldsymbol{\omega}_{BE}^B$ ,  $\Delta$  can be designed as

$$\Delta(\sigma_{BV}, \boldsymbol{\omega}_{EI}^B) = \begin{cases} k_e(\Gamma - V), & \Gamma > V \\ 0, & \Gamma \leq V \end{cases} \quad (25)$$

##### 4.1.1. Pointing constraint

The geometric relationship about the pointing constraint is displayed in Fig. 2, where  $\vartheta_e \in (0, \frac{\pi}{2})$  is the safety margin of  $\sigma_{BV}^B$  and satisfies  $\vartheta_e = \vartheta_m - \vartheta$ . When the body frame is coincided with the reference frame  $\mathcal{F}_V$ , the pointing angle  $\bar{\vartheta}$  is denote by

$$\bar{\vartheta} = \arccos(\overline{\mathbf{r}}_c^V \cdot \mathbf{r}_t^V) \quad (26)$$

Note that  $\overline{\mathbf{r}}_c^V = \mathbf{r}_c^B$  is a virtual constant unit vector expressed in  $\mathcal{F}_V$  rather than  $\overline{\mathbf{r}}_c^V = \mathbf{C}_B^V \mathbf{r}_c^B$ . Under these conditions, the safety margin of  $\sigma_{VI}^V$  satisfies  $\bar{\vartheta}_e = \vartheta_m - \bar{\vartheta}$  and  $\bar{\vartheta}_e \in (0, \frac{\pi}{2}]$ . Let  $\alpha \in [0, \pi]$  be the gap between  $\mathbf{n}_{BV}$  and the unit vector  $\mathbf{r}_c^B$ , then it satisfies

$$\mathbf{r}_c^B \cdot \mathbf{n}_{BV} = \cos(\alpha) \quad (27)$$

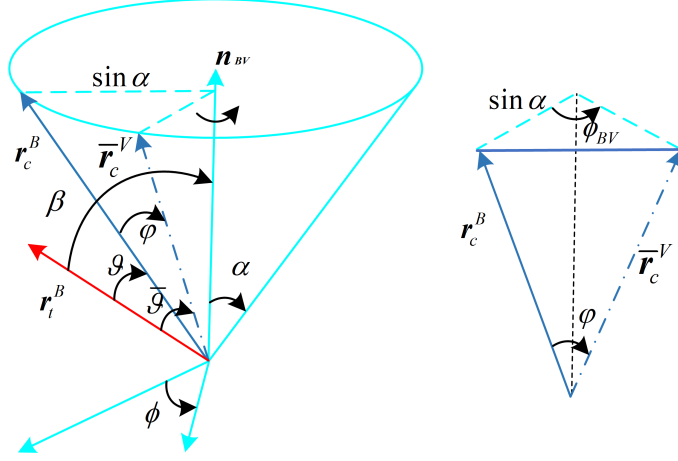


Figure 2: Constrained attitude region.

Let  $\varphi \in (0, \pi)$  denote the orientation from  $\mathbf{r}_c^B$  to  $\overline{\mathbf{r}}_c^V$ , and they have the following relationship:

$$\sin\left(\frac{\varphi}{2}\right) = \sin\left(\frac{\phi_{BV}}{2}\right)\sin(\alpha) \quad (28)$$

Obviously, there is a positive correlation between  $\varphi$  and  $\phi_{BV}$ , and they satisfies  $\varphi \leq \phi_{BV}$ . Since  $|\vartheta_e - \bar{\vartheta}_e| \leq \varphi$ , if  $\varphi \leq \bar{\vartheta}_e$ , then  $\vartheta_e \geq 0$  can be guaranteed.

According to [7], if  $\boldsymbol{\omega}_{EI}^E = \mathbf{0}_{3 \times 1}$  ( $\boldsymbol{\omega}_{BI}^B$  is precisely known), then  $\dot{V}_c = \dot{V} \leq 0$ , the threshold of  $V \leq \Gamma'_p$  can be designed as

$$\Gamma'_p = \begin{cases} 2k_p \ln \left\{ 1 + \left( \frac{1 - \sqrt{1 - a_p^2}}{a_p} \right)^2 \right\} & \alpha \in (0, \pi) \\ \infty & \alpha = 0 \text{ or } \pi \end{cases} \quad (29)$$

where  $a_p = \sin\left(\frac{\bar{\vartheta}_e}{2}\right)/\sin(\alpha)$ .

When  $V = \Gamma'_p$ ,  $\dot{\sigma}_{VI} = \mathbf{0}_{3 \times 1}$ . According to **Theorem 1**, the time derivate of  $V$  and  $\Gamma'_p$  satisfies  $\dot{V} \leq 0, \dot{\Gamma}'_p = 0$ , which means the pointing constraint (6) will never be violated. However,  $\boldsymbol{\omega}_{BI}^B$  and  $\delta_z$  are unavailable, which means  $V$  and  $V_c$  are unavailable, thus they can not be used to design the threshold of the pointing constraint. Hence, we approximate the Lyapunov function  $V$

with the following form

$$\bar{V} = 2k_p \ln(1 + \sigma_{BV}) + \frac{1}{2}(\boldsymbol{\omega}_{EI}^B)^T \mathbf{J} \boldsymbol{\omega}_{EI}^B \quad (30)$$

Although  $\dot{\bar{V}}$  is sign indefinite, according **Theorem 1**,  $\bar{V}$  is asymptotically convergent, i.e.,  $\lim_{t \rightarrow \infty} \bar{V}(t) = 0$ . Accordingly, the threshold of the pointing constraint is designed as

$$\Gamma_p = \frac{\Gamma'_p}{r^{k_1}} \quad (31)$$

where  $k_1 > 0$  is a constant parameter. Similarly to the analysis in Sec. 3.1, the larger  $\boldsymbol{\omega}_{BE}^B$  is, the larger  $r$  is, and the smaller  $\Gamma_p$  is. Although the exact relationship between  $\boldsymbol{\omega}_{BE}^B$  and  $r$  is unknown, by tuning  $k_1$ , a conservative but safe threshold of the pointing constraint without angular velocity measurement can be obtained.

#### 4.1.2. Angular velocity constraint

The angular velocity constraint given in (7) is a convex set. As discussed in Sec. 4.1.1, when  $\boldsymbol{\omega}_{EI}^E = \mathbf{0}_{3 \times 1}$ , the threshold of the angular velocity constraint  $\Gamma_\omega$  can be selected as

$$\Gamma'_\omega = \frac{1}{2} J_m \omega_{\max}^2 \quad (32)$$

Similar to the pointing constraint, when  $V = \Gamma'_\omega$ ,  $\dot{\sigma}_{VI} = \mathbf{0}_{3 \times 1}$ . Recalling **Theorem 1**, the time derivate of them satisfies  $\dot{V} \leq 0, \Gamma'_\omega = 0$ , which means the angular velocity constraint (7) will never be violated. When  $\boldsymbol{\omega}_{EI}^E \neq \mathbf{0}_{3 \times 1}$ , the Lyapunov function is approximate by (30), and the threshold can be selected as

$$\Gamma_\omega = \frac{\Gamma'_\omega}{r^{k_2}} \quad (33)$$

where  $k_2 > 0$  is a constant parameter used to tuning  $\Gamma_\omega$ .

#### 4.1.3. Actuator saturation

Similar to the preceding constraints,  $\boldsymbol{\omega}_{BI}^B$  is substituted with  $\boldsymbol{\omega}_{EI}^B$  and we omit the estimation error. Adhering to the approach outlined in [22], the saturation constraint (8) can be satisfied by solving the subsequent optimization problem

**Problem**

$$\min 2k_p \ln(1 + \sigma_{BV}) + \frac{1}{2}(\boldsymbol{\omega}_{EI}^B)^T \mathbf{J} \boldsymbol{\omega}_{EI}^B$$

subject to

$$|\boldsymbol{\sigma}_{BV}|_i \leq 1 \quad (34a)$$

$$|k_p \boldsymbol{\sigma}_{BV} + k_d \boldsymbol{\omega}_{EI}^B|_i \geq \tau_{\max} \quad (34b)$$

Then the threshold  $\Gamma_\tau$  can be obtained by selecting the minimum value from the aforementioned optimization problem for  $i = 1, 2, 3$ . Consequently, the upper-bound of the system subject to the constraint (9) can be concluded as  $\Gamma = \min\{\Gamma_p, \Gamma_\omega, \Gamma_\tau\}$ , a conclusion that can be substantiated by employing the same arguments presented in [21].

#### 4.2. Navigation layer

The navigation field  $\chi(\sigma_{VI}, \sigma_{VD})$  will be designed in this section to ensure that the auxiliary reference  $\boldsymbol{\sigma}_{BV}$  towards to the desired reference  $\boldsymbol{\sigma}_{BD}$ . Consequently, the trajectory of  $\chi(\sigma_{VD})$  must strictly align within the permissible set  $\mathcal{C}$ . Given that both the initial and final attitudes fall within the constraints and the pointing constraint  $\mathcal{C}_p$  constitutes a convex set, the shortest distance on the attitude manifold adheres to the constraints. The navigation trajectory  $\chi(\sigma_{VD})$  is designed by

$$\chi(\sigma_{VD}) = -G(\boldsymbol{\sigma}_{VD})\boldsymbol{\sigma}_{VD} \quad (35)$$

Since  $\boldsymbol{\omega}_{BI}^B = \mathbf{0}_{3 \times 1}$  and  $\boldsymbol{\tau}_c^B = \mathbf{0}_{3 \times 1}$  represent the equilibrium point, the constraints (7) and (8) are always satisfied at steady-state. Then, the main results about the constrained attitude maneuver control without angular velocity measurement is presented in the following proposition.

**proposition 2.** *Given the spacecraft attitude dynamics (1) subject to the constraints (9) with the angular velocity observer (12) controlled by (18), and let (24) be the navigation layer subject to the dynamic safety margin (25), and the navigation field (35). Then, for any initial states satisfy the constraints and  $V(0) \leq \Gamma(0)$ , the following statements hold. 1) For any constant reference  $\boldsymbol{\sigma}_{DI} \in \mathcal{C}$ , the system constraints are all satisfied. 2) The auxiliary reference  $\boldsymbol{\sigma}_{VI}$  updated by (24) asymptotically converges to  $\boldsymbol{\sigma}_{DI}$ .*

**Proof:** See [7]. ■

**Remark 2.** By integrating the ERG design process with the aforementioned analysis, it can be seen that by designing a trajectory from the current state to the final state that satisfies the constraint conditions, and then the controller drives the system state and the reference state error within a certain

range, the system states can be guaranteed to reach the target state while the constraints are met. An additional advantage of this strategy lies in its capability to maintain effective control even in the absence of state constraints. In comparison to alternative control algorithms like PID, the ERG algorithm can track the  $\sigma_{VD}$  independently generated by the reference management with smaller error than  $\sigma_{BD}$ . This capability leads to improved control performance characterized by enhanced speed and precision.

## 5. Numerical simulations

This section aims to demonstrate the effectiveness of the proposed angular velocity free attitude control algorithm in the presence of multi-constraints. The objective involves maneuvering the rigid spacecraft from a specific initial state to a pre-defined target, incorporating considerations for attitude constraints, angular velocity constraints, and control saturation concurrently. Besides, Monte Carlo results are conducted to further verify the robustness of the proposed control scheme. The inertia of the spacecraft is given by

$$\mathbf{J} = \begin{bmatrix} 15.2 & -1 & 2 \\ -1 & 18.3 & -0.5 \\ 2 & -0.5 & 16.1 \end{bmatrix} \text{ kg.m}^2.$$

The initial states are set as  $\boldsymbol{\sigma}_{BI}(0) = [-0.119, 0.000, 0.159]^T$  and  $\boldsymbol{\omega}(0) = [0, -0.01, 0.01]^T$  rad/s. The constraint conditions and target state are chosen in Table 1. Besides, the threshold of actuator saturation  $\Gamma_\tau$  is obtained by solving from the *Problem* via *fmincon* function in Matlab 2021, which is 0.0468, and the observer parameters are shown in Table 2. The control elements are selected as  $k_p = 1.5$  and  $k_d = 2.5$ . For the brevity and intuition, Euler angles  $[\varphi, \vartheta, \psi]^T$  with sequence 3 – 1 – 2 are used to plot the attitude.

### 5.1. Performance of the proposed control scheme

The simulation results are depicted in Figs. 3 – 11, where the dash curves illustrate the simulations conducted without reference management i.e., the constraints are not integrated into the control scheme. The attitude trajectories and angular velocities depicted in Figs. 3 and 4 indicate that with the navigation layer, the trajectories of attitude and the velocity become smoother and the overshoot is smaller.

Fig. 5 illustrates the attitude and angular velocity estimation errors generated by the I&I based observer designed in (12)–(17). In the logarithmic

Table 1: System Constraint Conditions.

Parameters	Values
$\sigma_{DI}$	$[0, 0, 0]^T$
$\vartheta_m$	$38^\circ$
$\mathbf{r}_t^I$	$[1/\sqrt{3}, -1/\sqrt{3}, 1/\sqrt{3}]^T$
$\mathbf{r}_c^B$	$[0, -1/\sqrt{2}, 1/\sqrt{2}]^T$
$\omega_{max}$	$0.035\text{rad/s}$
$\tau_{max}$	$0.1 \text{ N.m.s}$
$k_e$	$1000$
$k_1, k_2$	$2$

Table 2: Observer parameters.

Parameters	Values
$J_m$	$18.3$
$J_M$	$15.2$
$\rho_\sigma, \rho_\omega, \rho_{\underline{\omega}}, \rho_r, \varepsilon_\omega$	$0.1$
$r(0)$	$1$
$\xi(0)$	$[0, 0, 0]^T$
$\sigma_{EI}(0)$	$[-0.119, 0.000, 0.159]^T$
$\omega_{EI}^B$	$[0, 0, 0]^T \text{ rad/s}$

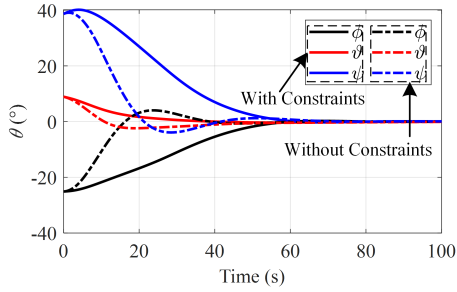


Figure 3: Attitude trajectories.

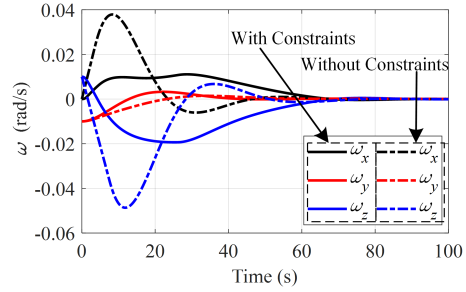


Figure 4: Angular velocities.

scale, the estimation errors  $\|\omega_{BE}^B\|$  and  $\|\sigma_{BE}\|$  decreases in an almost straight line, indicating that the estimation errors are exponentially convergent. An intriguing observation arises: unlike  $\|\omega_{BE}^B\|$  decreases consistently over time,

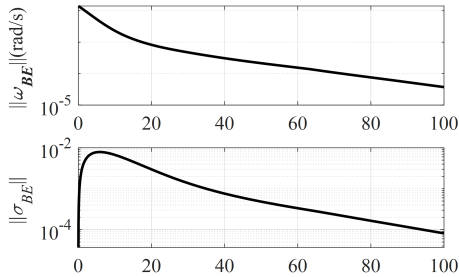


Figure 5: Attitude and velocity estimation errors.

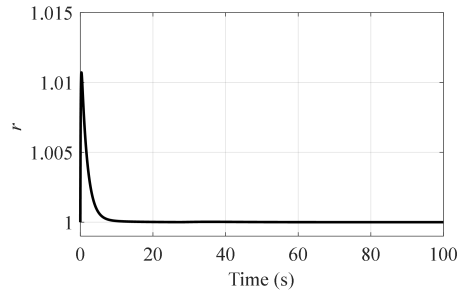


Figure 6: Injection gain  $r$ .

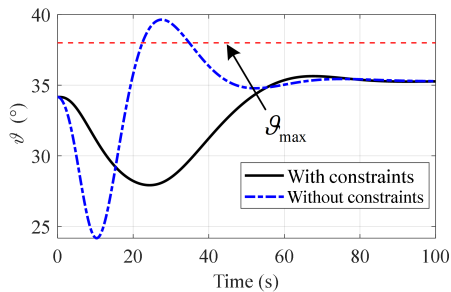


Figure 7: Pointing constraint.

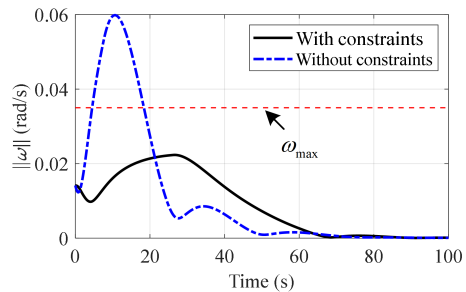


Figure 8: Angular velocity constraint.

$\|\sigma_{BE}\|$  initially remains very small but undergoes an initial increase before subsequently decreasing. This behavior arises because  $\|\sigma_{BE}\|$  is utilized as an "indicator" to assess the adequacy of the estimation of  $\|\omega_{BE}^B\|$ . As we set  $\|\sigma_{BE}\| = 0$  as the initial condition, and the estimation error  $\|\omega_{BE}^B(0)\|$  is substantial,  $\|\sigma_{BE}\|$  grows initially. As  $\|\omega_{BE}^B\|$  diminishes,  $\|\sigma_{BE}\|$  subsequently adjusts accordingly. As we can also see from Figs. 5 and 6, due to the large estimation error at the beginning, the injection gain  $r$  is also relatively large, but as the estimation error diminishes,  $r$  swiftly converges towards 1. These outcomes underscore the pivotal role of the injection gain  $r$  in the observer system, contributing significantly to achieving the desired effectiveness of the observer. Furthermore, the final angular velocity estimation error  $\|\omega_{BE}^B(0)\|$  measures approximately  $10^{-4}$ , which is mainly restricted by the simulation setting 0.01s. If the step size is further reduced,  $\|\omega_{BE}^B(0)\|$  can also be reduced.

The pointing constraint, angular velocity constraint and the control torque limitation are plotted in Figs. 7 – 9. Evidently, in the absence of reference

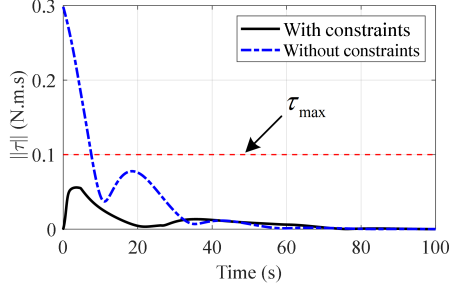


Figure 9: Control torque limitation.

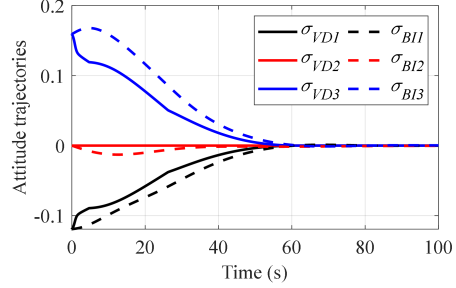


Figure 10: Reference trajectories.

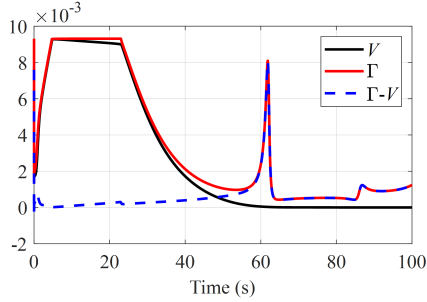


Figure 11: Threshold value.

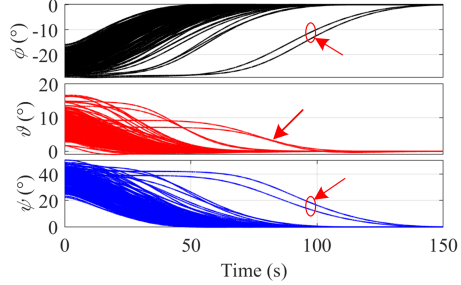


Figure 12: Attitude trajectories.

management, the pointing angle exceeds the boundary at 23 seconds, the angular velocity surpasses the limitation around 15 seconds, and the actuator saturation occurs within the initial 10 seconds. Upon the implementation of the navigation layer within the system, all three constraints remain within permissible bounds. This is because the tracking error can always maintain a small error relative to the reference trajectories (see Fig. 10). Analyzing Figs. 10 and 11, reveals that the convergence speed of the reference trajectory aligns closely with the threshold error  $\Gamma - V$ . Overall, the simulation results are in line with the theoretical analysis, verifying the effectiveness of the algorithm.

### 5.2. Monte Carlo simulation under disturbances

The aforementioned section presented numerical simulations without any disturbance i.e.,  $\tau_d = \mathbf{0}_{3 \times 1}$ . This section conducts Monte Carlo simulations encompassing disturbances to showcase the robustness of the proposed ERG and I&I technology-based attitude control scheme. To conduct the Monte Carlo simulations, randomized initial conditions and parameters are

detailed in Table 3. These newly introduced initial states and parameters are integrated with previously selected simulation conditions mentioned in the previous section, amounting to a total of 200 Monte Carlo simulations. In order to ensure that all the cases can reach the final states, those cases that do not meet the constraints at the initial moment will be excluded, and the simulations last for 150 seconds. Besides, the external disturbances are given as follows

$$\boldsymbol{\tau}_d^I = \left( \begin{bmatrix} 2 \\ -1 \\ -3 \end{bmatrix} + \begin{bmatrix} 0.4\sin(\omega_{At} + 1.6) \\ 2\sin(\omega_{At} + 1.1) \\ 0.7\sin(\omega_{At} - 2.1) \end{bmatrix} \right) \times 10^{-5} \text{N.m}^2$$

where  $\omega_{At} = 0.01 \text{rad/s}$ .

Figs. 12 and 13 depict the attitude and angular velocity trajectories of Monte Carlo simulations. Despite external disturbances and angular velocity estimation errors influencing the control performance, the spacecraft achieved the desired state smoothly. It can be seen from (12) and (13) that the precision of the input torque significantly influences estimation errors. In the Monte Carlo simulations, the presence of unknown disturbances results in slightly larger estimation errors, as depicted in Figs. 14 and 15, compared to those in Fig. 5. Nevertheless, these errors remain comparatively small, affirming the observer's robustness as designed in (12). Besides, the three constraints are basically satisfied during the simulation (see Figs. 16 – 18). Meanwhile, one can also see that the angular velocity observer is independent of the controller. No matter what constraints the system needs to meet, the observer can converge without being affected by them. This intriguing property enables us to enhance the ERG-based constrained controller without limitations imposed by the observer.

However, a slight setback is identified as there are two cases of slow convergence (as denoted by the red circles in Figs. 12, 13, 16, and 17). This occurrence is due to these specific cases being at the verge of the pointing constraint initially. Due to external disturbances and angular velocity estimation errors, the pointing angle slightly overflows the boundary. Fortunately, the algorithm designed in this study addresses these effects by employing an enhanced safety margin as described in (25), swiftly reeling back the pointing angle. To prevent such occurrences rigorously, adjusting the reference

Table 3: Randomized initial states and parameters.

Variables	Ranges
$\mathbf{n}(0)$	$[-0.7, -0.5] \times [-0.1, 0.1] \times [0.7, 0.9]$
$\phi(0)$ , rad	$[0.15\pi, 0.35\pi]$
$\boldsymbol{\omega}(0)$ , rad/s	$\{[-2, 2] \times [-2, 2] \times [-2, 2]\} \times 10^{-3}$
$J_m$	$[13, 17]$
$J_M$	$[15, 21]$
$k_p = 1.5$	$[1, 1.5]$
$k_d = 2.5$	$[2.5, 3.0]$
$k_e = 1000$	$[900, 1100]$

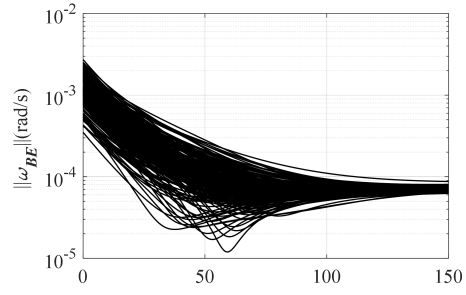
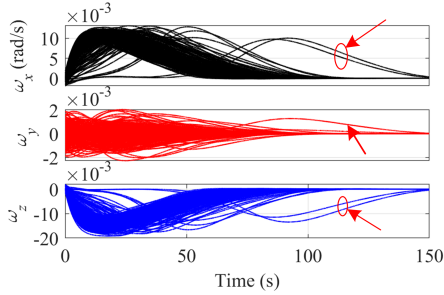


Figure 13: Angular velocity trajectories. Figure 14: Angular velocity estimation errors.

state’s margin suffices, a topic to be extensively explored in our subsequent research. In spite of this, the proposed ERG-based constrained controller still accomplished the maneuver objective with remarkable accuracy, which in turn demonstrates its robustness against uncertainties.

## 6. Conclusion

This paper develop a constrained output feedback attitude reorientation problem via ERG and I&I technologies, where pointing constraint, angular velocity constraint, and the control saturation are considered. The stability of a angular velocity observer and the output feedback controller is roughly proved. The inner loop of ERG is conducted by the angular velocity observer-based output feedback controller, and the navigation layer is designed by manipulating the auxiliary reference state without violating the constraints

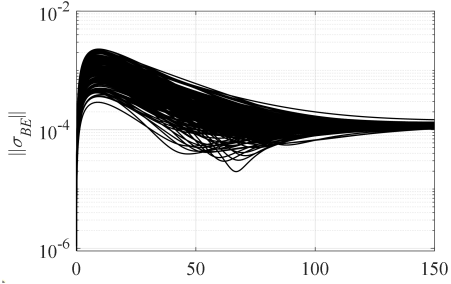


Figure 15: Attitude estimation errors.

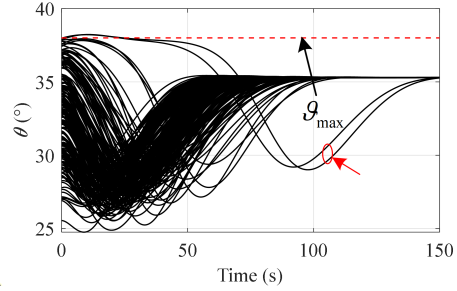


Figure 16: Distributions of pointing angles.

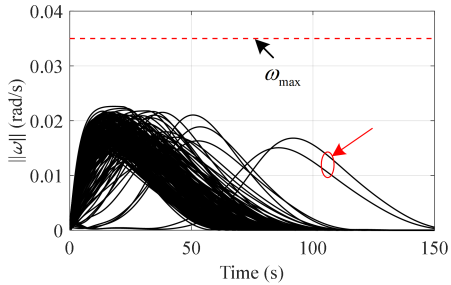


Figure 17: Distributions of angular velocity constraints.

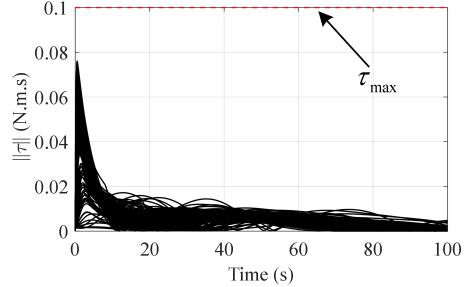


Figure 18: Distributions of control torque constraints.

while asymptotically converges to the desired reference. The performance of the proposed angular velocity observer and the ERG is meticulously analyzed and discussed by numerical simulations in detail.

## Acknowledgments

This work was partially supported by National Natural Science Foundation of China under grants 62273240, the Natural Science Foundation of Shaanxi Province (Grant No. 2023-JC-QN-0003), the Fundamental Research Funds for the Central Universities(Grant No. 23GH020210), Suzhou Municipal Science and Technology Bureau under Grant (ZXL2023177), and the basic Research Program of Taicang, Grant (TC2023JC13).

## Conflict of interest

The authors declare no potential conflict of interests.

## Declaration of generative AI and AI-assisted technologies in the writing process

During the preparation of this work the authors used ChatGPT in order to improve language and readability. After using this tool, the authors reviewed and edited the content as needed and take full responsibility for the content of the publication.

## Appendix A. Proof of proposition1

**Proof:** The **proposition1** can be proven by Lyapunov method by two steps. This first step is prestabilizing the inject estimation error  $\mathbf{z}$ . The second step is ensuring the dynamic scaling  $r$  is bounded.

The Lyapunov function candidate about the  $\mathbf{z}$  is chosen as

$$V_z = \frac{1}{2} \mathbf{z}^T \mathbf{J} \mathbf{z}. \quad (\text{A.1})$$

The dynamics of  $\boldsymbol{\omega}_{EI}^B$  can be obtained from (12), (13a), (14) that

$$\dot{\boldsymbol{\omega}}_{EI}^B = \mathbf{J}^{-1}(-\boldsymbol{\omega}_{EI}^B \times \mathbf{J} \boldsymbol{\omega}_{EI}^B + \boldsymbol{\tau}_c^B) + 4\mathbf{J}^{-1}\beta(\underline{\varpi})\dot{\boldsymbol{\sigma}}_{2BE}. \quad (\text{A.2})$$

One can derive the dynamics of  $\boldsymbol{\omega}_{BE}^B$  from (1b), (10b) , and (A.2) that

$$\dot{\boldsymbol{\omega}}_{BE}^B = \mathbf{J}^{-1}(\boldsymbol{\omega}_{EI}^B \times \mathbf{J} \boldsymbol{\omega}_{EI}^B - \boldsymbol{\omega}_{BI}^B \times \mathbf{J} \boldsymbol{\omega}_{BI}^B) - 4\mathbf{J}^{-1}\beta(\underline{\varpi})\dot{\boldsymbol{\sigma}}_{2BE}. \quad (\text{A.3})$$

Then, by invoking (5), (16) (17a), and (17b) and using the inequalities  $\|\boldsymbol{\omega}_{EI}^B\| \leq \underline{\varpi}$ ,  $\|\mathbf{a}\| \leq \|\mathbf{a} - \mathbf{b}\| + \|\mathbf{b}\|$ , and  $2\mathbf{a}\mathbf{b} \leq \|\mathbf{a}\|^2 + \|\mathbf{b}\|^2$ , the time derivative of  $V_z$  along (15) and (A.3) can be obtained as

$$\begin{aligned} \dot{V}_z &= \mathbf{z}^T \mathbf{J} r^{-1} \mathbf{J}^{-1} (\boldsymbol{\omega}_{EI}^B \times \mathbf{J} \boldsymbol{\omega}_{EI}^B - \boldsymbol{\omega}_{BI}^B \times \mathbf{J} \boldsymbol{\omega}_{BI}^B) \\ &\quad - \mathbf{z}^T \mathbf{J} \{ r^{-1} 4\mathbf{J}^{-1} \beta(\underline{\varpi}) \dot{\boldsymbol{\sigma}}_{2BE} - \dot{r}^{-1} \boldsymbol{\omega}_{BE}^B \} \\ &\leq \mathbf{z}^T (\boldsymbol{\omega}_{EI}^B \times \mathbf{J} \mathbf{z} - \underline{\beta}(\underline{\varpi}) \mathbf{z}) - r^{-1} \mathbf{z}^T \mathbf{J} \dot{r} \mathbf{z} \\ &\leq J_M \|\underline{\varpi}\| \|\mathbf{z}\|^2 - \underline{\beta}(\underline{\varpi}) \|\mathbf{z}\|^2 + \frac{J_m k_r}{J_M} \|\mathbf{z}\|^2 \\ &= - (1 + \rho_{\underline{\varpi}}) \|\mathbf{z}\|^2 \end{aligned} \quad (\text{A.4})$$

which implies  $\mathbf{z}$  converges to zeros exponentially.

To show the boundedness of  $\mathbf{r}$ , consider

$$V_o = V_z + V_{\underline{\varpi}} + V_{\sigma} + V_r \quad (\text{A.5})$$

where

$$\begin{aligned} V_\varpi &= \frac{1}{2}(\varpi - \underline{\varpi})^2 \\ V_\sigma &= 2\ln(1 + \sigma_{BE}^2) \\ V_r &= \frac{J_m}{2}(r - 1)^2. \end{aligned}$$

Using (11) and (A.2), the dynamics of  $\varpi$  is derived as

$$\begin{aligned} \dot{\varpi} &= \varpi^{-1}(\boldsymbol{\omega}_{EI}^B)^T \dot{\boldsymbol{\omega}}_{EI}^B \\ &= \varpi^{-1}(\boldsymbol{\omega}_{EI}^B)^T \mathbf{J}^{-1} \{ -\boldsymbol{\omega}_{EI}^B \times \mathbf{J} \boldsymbol{\omega}_{EI}^B + \boldsymbol{\tau}_c^B + 4\beta(\underline{\varpi}) \dot{\boldsymbol{\sigma}}_{2BE} \}. \end{aligned} \quad (\text{A.6})$$

From (13b) and (A.6), it follows that

$$\dot{\varpi} - \underline{\dot{\varpi}} = \varpi^{-1}(\boldsymbol{\omega}_{EI}^B)^T 4\mathbf{J}^{-1} \beta(\underline{\varpi}) \dot{\boldsymbol{\sigma}}_{2BE} - K_{\underline{\varpi}}(\varpi - \underline{\varpi}) \quad (\text{A.7})$$

Take the time derivative of  $V_\varpi$  along (A.7), one can obtain

$$\begin{aligned} \dot{V}_\varpi &= (\varpi - \underline{\varpi}) \{ \varpi^{-1}(\boldsymbol{\omega}_{EI}^B)^T 4\mathbf{J}^{-1} \beta(\underline{\varpi}) \dot{\boldsymbol{\sigma}}_{2BE} - K_{\underline{\varpi}}(\varpi - \underline{\varpi}) \} \\ &\leq \frac{1}{2} \mathbf{z}^2 - (\varpi - \underline{\varpi})^2 \left\{ K_{\underline{\varpi}} - 8 \left( \frac{\|\boldsymbol{\omega}_{EI}^B\| \beta(\underline{\varpi}) r}{J_m \varpi} \right)^2 \right\} \end{aligned} \quad (\text{A.8})$$

Applying (14) and (4), one has

$$\begin{aligned} \dot{V}_\sigma &= \frac{4\boldsymbol{\sigma}_{BE}^T}{1 + \sigma_{BE}^2} G(\boldsymbol{\sigma}_{BE}) (\boldsymbol{\omega}_{BE}^B - K_\sigma \boldsymbol{\sigma}_{BE}) \\ &\leq \frac{1}{2} \mathbf{z}^2 - \left( K_\sigma - \frac{1}{2} r^2 \right) \|\boldsymbol{\sigma}_{BE}\|^2 \end{aligned} \quad (\text{A.9})$$

Additionally, following the calculations in (16), one can obtain

$$\begin{aligned} \dot{V}_r &= J_m(r - 1) \left\{ \frac{r}{J_m} (J_M \|\varpi - \underline{\varpi}\|) - \frac{k_r}{J_M} (r - 1) \right\} \\ &\leq \frac{1}{2} \mathbf{r}^2 J_M \|\varpi - \underline{\varpi}\|^2 - \left( \frac{J_m k_r}{J_M} - \frac{1}{2} J_M \right) (r - 1)^2 \end{aligned} \quad (\text{A.10})$$

Finally, differentiating  $V_o$  along (A.4), (A.8), (A.9), and (A.10), yields

$$\dot{V}_o \leq -\rho_\varpi \|\mathbf{z}\|^2 - \rho_{\underline{\varpi}} (\varpi - \underline{\varpi})^2 - \rho_\sigma \|\boldsymbol{\sigma}_{BE}\|^2 - \rho_r (r - 1)^2 \quad (\text{A.11})$$

which implies that the system is exponentially stable and  $r$  is bounded. This completes the proof.

## References

- [1] C. Wei, Q. Chen, J. Liu, Z. Yin, J. Luo, An overview of prescribed performance control and its application to spacecraft attitude system, *Proceedings of the Institution of Mechanical Engineers, Part I: Journal of Systems and Control Engineering* 235 (4) (2021) 435–447.
- [2] R. Qi, X. Dong, D. Chao, Y. Wang, Constrained attitude tracking control and active sloshing suppression for liquid-filled spacecraft, *ISA Transactions* 132 (2023) 292–308.
- [3] S. Nakano, T. W. Nguyen, E. Garone, T. Ibuki, M. Sampei, Explicit reference governor on  $so(3)$  for torque and pointing constraint management, *Automatica* 155 (2023) 111103.
- [4] Y. Qu, X. Zhong, F. Zhang, X. Tong, L. Fan, L. Dai, Robust disturbance observer-based fast maneuver method for attitude control of optical remote sensing satellites, *Acta Astronautica* 201 (2022) 83–93.
- [5] H. B. Hablani, Attitude commands avoiding bright objects and maintaining communication with ground station, *Journal of Guidance, Control, and Dynamics* 22 (6) (1999) 759–767.
- [6] H. Cui, X. Cheng, Anti-unwinding attitude maneuver control of spacecraft considering bounded disturbance and input saturation, *SCIENCE CHINA Technological Sciences* 55 (9) (2012) 2518–2529.
- [7] Q. Dang, K. Liu, J. Wei, Explicit reference governor based spacecraft attitude reorientation control with constraints and disturbances, *Acta Astronautica* 190 (2022) 455–464.
- [8] S. H. Pourtakdoust, M. F. Mehrjardi, M. Hajkarim, Attitude estimation and control based on modified unscented kalman filter for gyro-less satellite with faulty sensors, *Acta Astronautica* 191 (2022) 134–147.
- [9] J. Hu, H. Zhang, Bounded output feedback of rigid-body attitude via angular velocity observers, *Journal of Guidance, Control, and Dynamics* 36 (4) (2013) 1240–1248.
- [10] H. C. Kjellberg, E. G. Lightsey, Discretized constrained attitude pathfinding and control for satellites, *Journal of Guidance, Control, and Dynamics* 36 (5) (2013) 1301–1309.

- [11] B. Wie, D. Bailey, C. Heiberg, Rapid multitarget acquisition and pointing control of agile spacecraft, *Journal of Guidance Control Dynamics* 25 (1) (2002) 96–104.
- [12] Y. Cheng, D. Ye, Z. Sun, S. Zhang, Spacecraft reorientation control in presence of attitude constraint considering input saturation and stochastic disturbance, *Acta Astronautica* 144 (2018) 61–68.
- [13] S. Kulumani, T. Lee, Constrained geometric attitude control on  $so(3)$ , *International Journal of Control, Automation and Systems* 15 (6) (2017) 2796–2809.
- [14] B. Hua, J. He, H. Zhang, Y. Wu, Z. Chen, Spacecraft attitude reorientation control method based on potential function under complex constraints, *Aerospace Science and Technology* 144 (2024) 108738.
- [15] U. Lee, M. Mesbahi, Feedback control for spacecraft reorientation under attitude constraints via convex potentials, *IEEE Transactions on Aerospace and Electronic Systems* 50 (4) (2014) 2578–2592.
- [16] Q. Hu, B. Chi, M. R. Akella, Anti-unwinding attitude control of spacecraft with forbidden pointing constraints, *Journal of Guidance, Control, and Dynamics* 42 (4) (2019) 822–835.
- [17] Q. Shen, C. Yue, C. H. Goh, B. Wu, D. Wang, Rigid-body attitude stabilization with attitude and angular rate constraints, *Automatica* 90 (2018) 157 – 163.
- [18] U. V. Kalabić, R. Gupta, S. D. Cairano, A. M. Bloch, I. V. Kolmanovsky, MPC on manifolds with an application to the control of spacecraft attitude on  $SO(3)$ , *Automatica* 76 (2017) 293 – 300.
- [19] D. Y. Lee, R. Gupta, U. V. Kalabić, S. Di Cairano, A. M. Bloch, J. W. Cutler, I. V. Kolmanovsky, Geometric mechanics based nonlinear model predictive spacecraft attitude control with reaction wheels, *Journal of Guidance, Control, and Dynamics* 40 (2) (2017) 309–319.
- [20] M. M. Nicotra, E. Garone, The explicit reference governor: A general framework for the closed-form control of constrained nonlinear systems, *IEEE Control Systems Magazine* 38 (4) (2018) 89–107.

- [21] E. Garone, M. M. Nicotra, Explicit reference governor for constrained nonlinear systems, *IEEE Transactions on Automatic Control* 61 (5) (2016) 1379–1384.
- [22] M. M. Nicotra, D. Liao-McPherson, L. Burlion, I. V. Kolmanovsky, Spacecraft attitude control with nonconvex constraints: An explicit reference governor approach, *IEEE Transactions on Automatic Control* 65 (8) (2020) 3677–3684.
- [23] M. Hosseinzadeh, E. Garone, An explicit reference governor for the intersection of concave constraints, *IEEE Transactions on Automatic Control* 65 (1) (2020) 1–11.
- [24] M. Nicotra, E. Garone, Constrained control of nonlinear systems: The explicit reference governor and its application to unmanned aerial vehicles, Ph.D. thesis, Universite Libre de Bruxelles (2016).
- [25] B. Chi, Q. Hu, Saturated explicit reference governor for spacecraft constrained attitude reorientation control, *Aerospace Science and Technology* 145 (2024) 108874.
- [26] M. N. Hasan, Y. Chen, J. Liang, A. Wen, Fixed-time fault-tolerant attitude control for flexible spacecraft without angular velocity sensor, *ISA Transactions* (2023, in press).
- [27] S. Yang, M. R. Akella, F. Mazenc, Immersion and invariance observers for gyro-free attitude control systems, *Journal of Guidance Control Dynamics* 39 (11) (2016) 2567–2574.
- [28] E. Espíndola, Y. Tang, A new angular velocity observer for attitude tracking of spacecraft, *ISA Transactions* 130 (2022) 377–388.
- [29] R. Schlanbusch, E. I. Ingar Grotli, Hybrid certainty equivalence control of rigid bodies with quaternion measurements, *IEEE Transactions on Automatic Control* 60 (9) (2015) 2512–2517.
- [30] J. G. Romero, R. Ortega, I. Sarras, A globally exponentially stable tracking controller for mechanical systems using position feedback, *IEEE Transactions on Automatic Control* 60 (3) (2015) 818–823.

- [31] Q. Dang, H. Gui, H. Wen, Dual-quaternion-based spacecraft pose tracking with a global exponential velocity observer, *Journal of Guidance, Control, and Dynamics* 42 (9) (2019) 2106–2115.
- [32] Q. Shen, C. Yue, C. H. Goh, Velocity-free attitude reorientation of a flexible spacecraft with attitude constraints, *Journal of Guidance, Control, and Dynamics* 40 (5) (2017) 1293–1299.
- [33] J. L. Junkins, H. Schaub, *Analytical mechanics of space systems*, American Institute of Aeronautics and Astronautics, 2009.
- [34] H. Gui, G. Vukovich, Adaptive integral sliding mode control for spacecraft attitude tracking with actuator uncertainty, *Journal of the Franklin Institute* 352 (12) (2015) 5832 – 5852.
- [35] M. Diaz Ramos, H. Schaub, Kinematic steering law for conically constrained torque-limited spacecraft attitude control, *Journal of Guidance, Control, and Dynamics* 41 (9) (2018) 1990–2001.
- [36] A. Bemporad, Reference governor for constrained nonlinear systems, *IEEE Transactions on Automatic Control* 43 (3) (1998) 415–419.